IEEE Access
Multidisciplinary | Rapid Review | Open Access Journal

Received 29 October 2023, accepted 14 November 2023, date of publication 21 November 2023,
date of current version 1 December 2023.

Digital Object Identifier 10.1109/ACCESS.2023.3335653

RESEARCH ARTICLE

A Wideband Closed-Loop Residual Current Sensor Based on Self-Oscillating Fluxgate

ZHIWEN DING, JIAFU WANG, (Member, IEEE), CHUANSHENG LI, KUN WANG, (Member, IEEE), AND HAIMING SHAO, (Member, IEEE)
National Institute of Metrology, Beijing 100029, China

Corresponding authors: Haiming Shao (shaohm@nim.ac.cn) and Kun Wang (wang-kun@nim.ac.cn)

This work was supported by the National Key Research and Development Program of China under Grant 2023YFF0614803.

ABSTRACT The increasing switching frequency of inverters in new electric power technology causes leakage currents at tens or even hundreds of kHz, exceeding the measurement frequency range of conventional AC residual current sensors. In addition, the cost of residual current sensors developed specifically for DC is high, limiting further application promotion. Hence, this paper focuses on designing a wideband closed-loop residual current sensor based on self-excited oscillation fluxgate, which outperforms ordinary measurement methods. The sensor is developed through the optimization of demodulation circuits, and the increase of AC windings and the construction of excitation voltage regulating circuits. The DC residual current measurement accuracy of the sensor is better than ±0.2%. The standard deviation of zero-point change is 0.00046 mA. The adoption of this innovative sensor not only enables precise and stable measurement of residual currents but also facilitates current monitoring in high-frequency applications. It can be fully applied in the field of power technology and will promote the development of efficient and reliable power systems.

INDEX TERMS Self-oscillating, fluxgate, high frequency, residual current sensor, RC demodulation.

I. INTRODUCTION

With the development and safety improvement of electric power technology, the requirements for the accuracy and bandwidth of leakage current measurement are getting higher and higher, especially in the fields of new energy vehicles, wind energy storage, and smart factories where a large number of AC and DC converter circuits exist. These applications require inverters to invert DC voltage into frequency-adjustable AC to drive the motor, and during this process high frequency pulse voltage accelerates its insulation degradation [1]. The insulation degradation leading to the presence of wide frequency currents in the parasitic capacitance between the rotor and stator and the casing of the inverter motor [2], so the insulation performance of inverter motors can be evaluated and calculated by measuring the leakage current [3]. In addition, although the new transformer-less three-phase photovoltaic inverter makes progress in reducing size, weight and cost, the lack of electrical isolation leads to large leakage currents [4]. Considering that the inverter's switching frequency is 40 kHz, its poor grounding of the enclosure will cause induced leakage currents at low-frequency and high-frequency. In this case, most conventional residual current sensors have difficulty in meeting the requirements of wide-frequency measurements [5]. Wide-frequency current sensors, including Hall current sensors and Roche coils, usually have large measurement ranges and their accuracy decreases under milliamp residual current conditions [6], [7]. On the other hand, with the development of DC distribution systems, more power systems in the future adopt DC distribution [8], [9], [10], which has a simpler structure and lower power consumption compared with AC distribution systems [11]. At present, the measurement of DC residual current is still immature, and AC residual current sensors cannot meet the DC measurement requirements. The strength of fluxgate current sensors in stability, sensitivity, linearity, etc., makes them suitable for DC residual current measurement [6], [7], so in order to measure the wide-frequency, low-magnitude AC and DC residual currents with high accuracy, current sensors based on fluxgate are frequently adopted.

The associate editor coordinating the review of this manuscript and approving it for publication was Bo Pu.

Traditional fluxgate current sensors consist of high-frequency voltage excitation, analog switches and phase-sensitive demodulators [12], and their modulation principles include phase-difference magnetic modulation [13], [14], [15], frequency-doubling magnetic modulation, etc. [16], whose complex demodulation circuit structure and high cost limit their large-scale applications [17]; and air-gap fluxgate residual current sensors suffer from the complexity of the core structure and high cost, low sensitivity and other disadvantages. At the same time, the magnetic permeability of the core air gap differs greatly from that of other parts, resulting in a large eccentricity error of the sensor [18], which is also not suitable for residual current measurement. The measurement accuracy of DC residual current sensors, based on the fluxgate principle, is reported to reach up to ±0.1% [19], [20]. However, these sensors are limited in terms of measurement bandwidth. Typically, they can only handle current measurement at the milliampere level, with a bandwidth ranging from a few hundred to a few kilohertz [12], [21], [22]. Consequently, these sensors may not fully meet the requirements for conducting broadband residual current measurements.

In this paper, we propose a wideband closed-loop AC/DC residual current sensor based on self-excited oscillating fluxgate, with enhanced measurement bandwidth through AC winding in-crease. Moreover, the stability of the zero-point of the sensor is improved by adjusting the sensor excitation current and frequency, and the structure complexity and cost of the sensor are reduced through the optimization of the de-modulation circuit. The proposed scheme can meet the residual current measurement demands in the insulation performance evaluation process or online monitoring of inverter motors.

II. PROPOSED RESIDUAL CURRENT SENSOR DESIGN

The general design schematic of the closed-loop self-excited fluxgate residual current sensor is shown in Fig.1. The excitation current i_{E1} excites the magnetic core T_1 to an alternating saturation state through N_{E1}, and the measured current generates a magnetic potential bias, which then turns into a harmonic voltage V_E in the excitation loop. The harmonic voltage goes through a filter and an integrator and becomes the error voltage signal at the excitation frequency, which is then amplified by a power amplifier and transformed into the compensation current I_s. Afterwards, I_s passes through the compensation winding N_s to generate a magnetic flux Φ_s inside the magnetic core. A magnetic flux Φ_p(generated by the current i_P) of equal amplitude and opposite direction to Φ_s makes the total magnetic flux inside the magnetic core T_1 and T_2 zero, so $i_P = (I_s{*}N_s)$.

To ensure the stability of the sensor zero-point, the excitation voltage regulationmodule is applied to the sensor, which can adjust the amplitude of the excitation voltage precisely during the commissioning process, observe the dynamic changes in the zero-point, and optimize the magnetic core

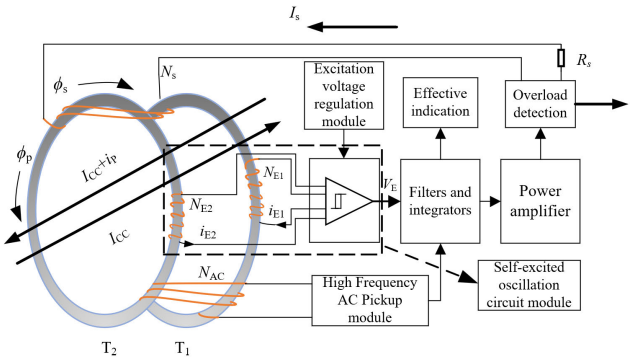

FIGURE 1. The schematic of closed-loop self-oscillating excitation fluxgate residual current sensor.

working condition. In addition, the overload detection module can be used to set up the action current value in accordance with the standard of the residual current sensor to ensure the safety of the circuit, and a light is utilized to indicate the working status of the sensor. The AC winding N_{AC}, high frequency AC pickup module, the integrator and the power amplifier module together form a wide-frequency current transformer, which finally turns into a system for wide-frequency residual current measurement. Since the fluxgate excitation circuit periodically saturates the coil, the transformer effect will be introduced into the measured end of the high-frequency noise [23]. The excitation current i_{E2} through the N_{E2} will be the magnetic core T_2 excitation to the alternating to compensate for the excitation current noise, which generates a magnetic flux inside the core of T_2 of equal magnitude and opposite direction to that of T_1, to cancel out the excitation current noise of T_1. The design scheme of each sub-module is described below.

A. EXCITATION CIRCUIT DESIGN

The excitation module consists of the magnetic core T_1 and T_2, the excitation winding N_{E1} and N_{E1}, and the Schmitt trigger. In order to ensure that the fluxgate sensor has good sensitivity, the designed excitation circuit must be able to keep the magnetic core in the oversaturation state, and the magnitude of the saturation current of excitation coil is an important factor affecting the saturation of the magnetic core [24]. The Schmitt trigger can generate positive and negative square wave signals by setting positive and negative threshold voltages, which drive the excitation coil into alternate saturation states through push-pull circuits.

Considering the linear approximation of the core B-H relationship, the excitation coil saturation current I_{sat} is defined as (1) [25]:

$$I_{sat} = \frac{H_{sat} l_e}{N_{E1}} \approx \frac{B_{sat} l_e}{\mu_0 \mu_r N_{E1}} \tag{1}$$

where B_{sat} is the core flux density saturation, l_e is the magnetic circuit length, μ_r is the relative permeability. A_e is the core cross-sectional area and the coil inductance L_s can be

TABLE 1. Core parameters.

Parameters	Numerical value
Outer diameter	52 mm
Inner diameter	46.8 mm
height	3 mm
B_{sat}	0.58 T
A_e	7.8 mm²
l_e	155.12 mm
N_{E1}	90

defined as [25]:

$$L_s = \frac{N_{E1}^2 \mu_0 \mu_r A_e}{l_e} \tag{2}$$

Generally, lower saturationcurrent and inductance can reduce the sensor size and power consumption, and lower the cost of the sensor. Since the current to be measured is small, the residual current sensor is required to possess high sensitivity. Consequently, the core with high relative permeability and small size should be selected for overall consideration.

The parameters that mainly influence the sensitivity of the sensor include the core permeability, the frequency of the excitation field, and the effective cross-sectional area of the core [24]. Nanocrystalline soft core materials are ideal for fluxgate current sensors owing to their high permeability, low power consumption and low coercivity [26]. In this paper, VITROVAC 6025 Z cobalt-based amorphous, which has a low saturation point (0.58 T), is chosen as the core material for low power consumption [27]. The core material has small coercivity and is also suitable for higher excitation frequency.

Based on the circuit characteristics of this scheme, the excitation frequency is set between 8 and 10 kHz, which is determined according to the fluxgate excitation current equation [24]:

$$f = \frac{V_H}{4B_{sat} N_{E1} A_e} \tag{3}$$

V_H is the amplitude of the excitation voltage.

The prototype is made from a core strip, which is wound along the circumference of the excitation coil skeleton. The excitation winding is made of 0.25 mm diameter enameled wire.

The specific parameter settings for the core material are shown in Table 1.

The self-excited oscillation circuit proposed in this paper is illustrated in Fig.2, V_z is the excitation voltage limit, so the maximum value of the excitation current when the core is positively saturated is:

$$I_{E+\,max} = \frac{V_z}{R_1 + R_E + R_3} \tag{4}$$

where R_E is the internal resistance of the excitation winding, and the negative saturation current $I_{E+\,min} = -I_{E+\,max}$.

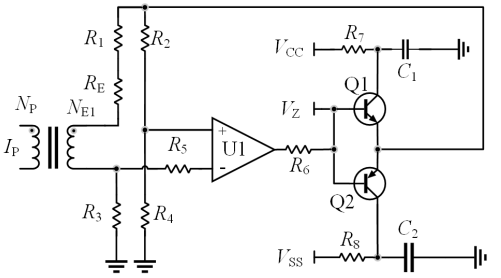

FIGURE 2. Self-excited oscillation circuit.

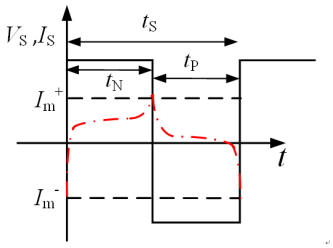

FIGURE 3. Signal modulation waveform.

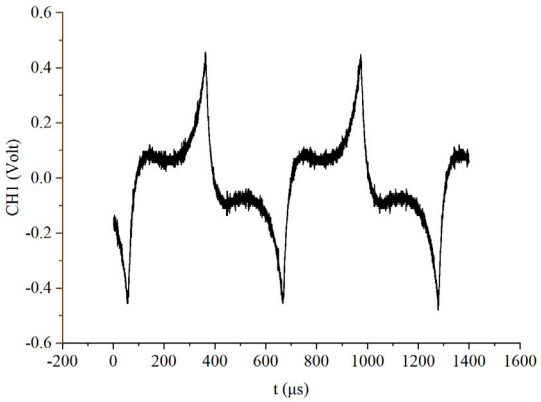

FIGURE 4. Excitation current waveforms during core operation.

According to KVL law the voltage equations for the unsaturated and post-saturated excitation loops are as follows:

$$V_{E1} = i_e(t)\,(R_1 + R_E + R_3) + L\frac{di_E(t)}{dt} \tag{5}$$

$$V_{E2} = i_e(t)(R_1 + R_E + R_3) + L_{sat}\frac{di_E(t)}{dt} \tag{6}$$

In the presence of the primary current i_p, and taking the positive saturation as an example, the excitation current is:

$$i_E^+ = I_{E+\,max} - i_p\frac{N_P}{N_S} \tag{7}$$

$$i_E^- = I_{E+\,min} - i_p\frac{N_P}{N_S} \tag{8}$$

Due to the injection of the measured current, the excitation coil saturates early or delayed in the positive and negative directions. Correspondingly, the excitation current waveform changes, so the average value in the cycle is no longer zero.

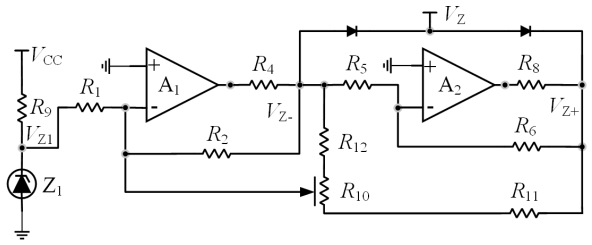

FIGURE 5. Excitation voltage regulation circuit.

Thus, the measured current completes the modulation as shown in Fig.3.

After the test sensor is energized, the waveforms when the magnetic core is working are shown in Fig 4. From the shape of the excitation waveform, it can be seen that the magnetic core oscillates repeatedly between the saturated and unsaturated state, which satisfies the conditions for normal operation of the magnetic core. The experimental waveform plots were drawn from the data sequence points obtained from the oscilloscope data sampling.

B. EXCITATION VOLTAGE REGULATION CIRCUIT

The magnetic core of the fluxgate current sensor is periodically saturated alternately, the size of the excitation current is an important factor affecting H, which directly leads to the degree of saturation of the hysteresis return line of the core material, and the excitation current can be adjusted by the excitation voltage, so the zero-point dynamic change of the sensor can be optimized by designing the excitation voltage regulation circuit to change the size and frequency of the excitation voltage. The design of the excitation voltage regulation circuit is shown in Fig. 5 (the zero-point dynamic change test is shown in Fig. 15).

The relationship between the magnetic field strength and the excitation current is:

$$H = \frac{N_{E1} I_{E1}}{l_e} \tag{9}$$

where H is the magnetic field strength; N_{E1} is the number of turns of the excitation coil; I_{E1} is the excitation current; and the magnetic field strength generated by the excitation current and the measured current is [24]:

$$H(t) = \frac{N_{E1}}{l_e}(I_P + i_S(t)) \tag{10}$$

In Fig.5 R_9 provides working current for Z_1 to acquire V_{Z1}, V_{Z1} is amplified by equal and inverse proportionality to acquire V_{Z-}, and since $R_5 = R_6$, $V_{Z+} = -V_{Z-}$. After R_{10} regulation feedback, V_Z changes as shown in (11).

$$V_Z = -V_{z1} \times \frac{R_2}{R_1} + (-v_{adj} \times \frac{R_2}{R_1}) \tag{11}$$

$$v_{adj} = \frac{2V_{z+}}{R_{12} + R_{11} + R_{10}} \times \left(\frac{1}{2} - \delta_{adj}\right) R_{10} \tag{12}$$

In (12), δ_{adj} is the relative ratio of the current adjustable resistor R_{10} to the full value. R_{10} adjustment can tune the magnitude of V_Z, and then control the magnitude of the excitation voltage through the limiting circuit. In this way, the dynamic control and adjustment of the sensor zero-point is achieved.

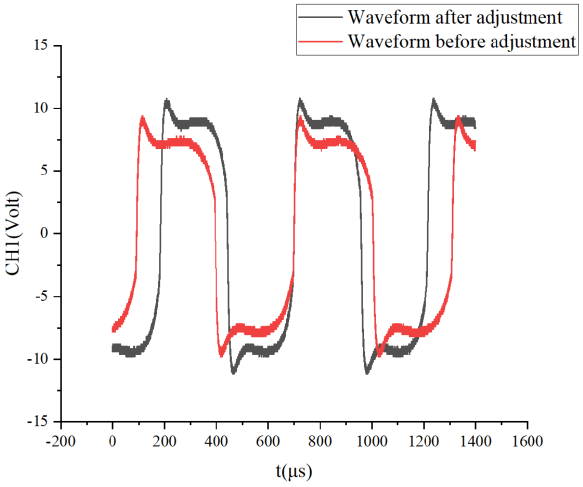

FIGURE 6. Excitation voltage regulation circuit effect diagram.

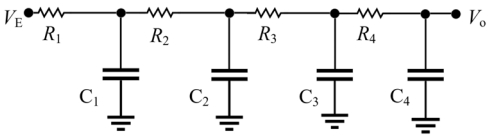

FIGURE 7. Integrator circuit.

The effect of excitation voltage regulation is shown in Fig. 6. The amplitude and frequency of the excitation voltage change after circuit regulation, this indicates that the excitation voltage regulation module is working properly and meets design expectations.

C. SECOND HARMONIC DEMODULATION

When the primary current I_p is not zero, the induced second harmonic voltage is linearly related to the primary current [28]. Therefore, the demodulation of the second harmonic is completed by integrating the excitation current to obtain the non-zero error voltage signal u_{DC}, which drives the power amplifier to generate a compensation current into the compensation winding to achieve a zero-flux state.

Currently there are various methods for demodulation of the second harmonic commonly used in flux gates, such as peak difference detector method, phase sensitive demodulation method and average current method [23], [29], [30]. In this paper, we adopt the relatively simple average current method and design a RC circuit for demodulation. which has a simple structure, strong anti-interference, favorable low frequency performance. The RC circuit can be composed of only resistive-capacitive components for reducing cost.

An integrator takes an input signal and integrates it, averaging to reject high-frequency noise while preserving

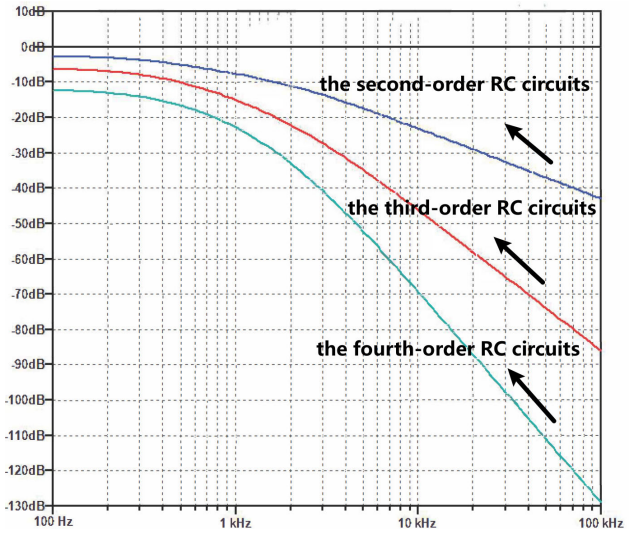

FIGURE 8. Simulation of RC filter integrator.

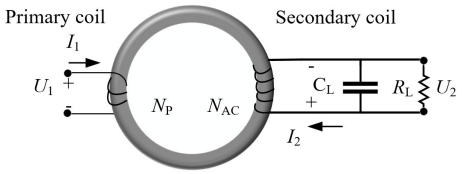

FIGURE 9. Principle of high-frequency current pickup.

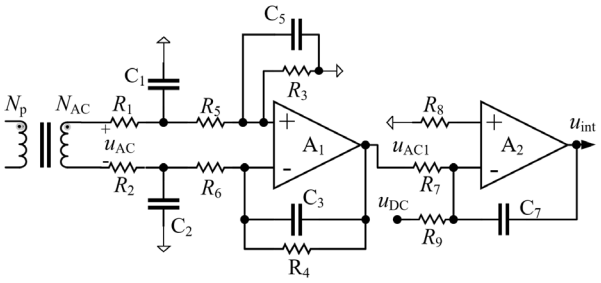

FIGURE 10. AC pickup circuit.

lower frequency signals [31], [32]. From this point of view, it is reasonable to consider the integrator as equivalent to a low-pass filter. The integrator used in this paper is shown in Fig. 7 and consists of four identical RC filters, which form a fourth-order RC integrator, R_1=R_2=R_3=R_4=R, C_1=C_2=C_3=C_4=C. The transfer function of the fourth-order RC integrator is given in (13):

$$\frac{V_o}{V_E} = \frac{1}{(j\omega RC)^4 + 7(j\omega RC)^3 + 15(j\omega RC)^2 + 10j\omega RC + 1} \tag{13}$$

Because the signal passing through the integrator needs to be used as a compensation current to cancel out the measured current, the attenuation of the high-frequency signal is more strictly controlled. As shown in Fig.8, through the simulation of the RC low-pass filter, it can be found that the attenuation values of the second-order, third-order and fourth-order RC circuits for the signal at 20 kHz (the second harmonic frequency) are 30 dB, 60 dB and 90 dB, respectively, and therefore the third-order and fourth-order RC low-pass filters are more in line with the design requirements.

D. AC PICKUP CIRCUIT AND BAND COMBINING INTEGRATORS

Current transformer is usually selected for high frequency residual current measurement, but it cannot be used for DC measurement [7]. Currently, the commercial high-frequency residual current sensors are only a simple integration of the current transformer as a second sensor, which cannot be used as a systematic current sensor. The entire measurement process is not in a zero-flux state, resulting in non-ideal accuracy. In this paper, the current transformer and the fluxgate current sensor are designed as a current measurement system by implementing an AC pickup circuit, which superimposes the high-frequency AC signal with the DC signal. The output signal is applied to the compensation circuit, in a closed loop for keeping the measurement process in the zero-flux state all the time.

The principle of high-frequency current transformer picking up high-frequency current is shown in Fig.9. According to the principle of electromagnetic induction, the transfer function from the current to be measured to the output voltage is [33]:

$$H(j\omega) = \frac{U_2}{I_1} = \frac{N_P}{N_{AC}} \cdot \left(\frac{1}{\frac{1}{R_L} + j\omega C_L + \frac{1}{\frac{j\omega (N_{AC})^2}{R}}} \right) \tag{14}$$

where R is the core reluctance.

The AC pickup circuit and band combining integrator are shown in Fig.10, which uses a differential amplifier circuit to pick up the high-frequency AC, effectively suppress the common-mode signals, and amplify the AC signals on the AC winding N_{AC}. The bandwidth of the AC pickup circuit is determined by the differential amplifier's Gain Bandwidth.

The low-frequency gain of the differential amplifier in Fig. 10 is:

$$G = \frac{u_{AC1}}{u_{AC}} = \frac{R_4}{R_2 + R_6} \tag{15}$$

The cutoff frequency f_{RC} of the differential amplifier on condition that f_{RC} is greater than the required bandwidth of the residual current sensor, is represented in (16).

$$f_{RC} = \frac{1}{2\pi R_2 C_2} \times \frac{1}{2\pi R_6 C_3} \tag{16}$$

The AC pickup circuit output signal u_{AC} and the second harmonic demodulation circuit output signal u_{DC} form a frequency band combining circuit with integrator A_2. The

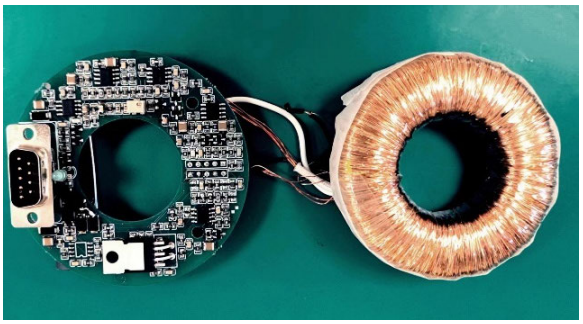

FIGURE 11. Designed sensor prototypes.

output signal u_{int} of the frequency band combining circuit is:

$$u_{int} = \frac{1}{R_7C_7}\int u_{AC1}dt + \frac{1}{R_9C_7}\int u_{DC}dt = \frac{1}{R_7C_7}\int \frac{R_4}{R_2+R_6}u_{AC}dt + \frac{1}{R_9C_7}\int u_{DC}dt \quad (17)$$

III. EXPERIMENTAL RESULTS

In this section, a fluxgate residual current sensor prototype is built according to the above proposed principles, as well as the adopted magnetic performance materials and size parameters. The multi experiments including AC, pulsating DC, multi-phase rectification and other residual current evaluation, linearity and accuracy evaluation, frequency response evaluation, response time evaluation for step change of the prototype conforms to the IEC/TR 60755 [34] and IEC 62752 [35] international standards. After experiments and analysis, the number of compensating coil turns is 50 turns and the sampling resistance is 20 ohms. The designed sensor prototype is shown in Fig. 11.

A. AC, PULSATING DC RESIDUAL CURRENT, MULTIPHASE RECTIFIED RESIDUAL CURRENT EVALUATION

According to the IEC/TR 60755 [34] standard, the sensor needs to be evaluated for residual current waveform testing. By applying pulsating DC residual current, two-phase rectified pulsating DC residual current, three-phase rectified pulsating DC residual current and high-frequency AC to the sensor, it can be seen that the sensor is able to reproduce the corresponding waveforms, and Fig.12 (a)(b)(c)(d) shows the sensor's responses to the test of pulsating DC residual current, two-phase rectified pulsating DC residual current, three-phase rectified pulsating DC residual current and high-frequency AC, respectively, which satisfy the requirements for residual current waveforms and frequencies.

B. FREQUENCY RESPONSE EVALUATION

This evaluation analyzes a small signal with the same magnitude 100 mA and sequentially increasing frequency, and measures the input and output voltage gain of the sensor under different frequencies. According to the evaluation results shown in Fig.13, the sensor has a 3 dB bandwidth over 100 kHz, which meets the requirements of 100 kHz residual currents in the IEC 62752-2016 standard, and suitable for the measurement of high-frequency residual currents.

TABLE 2. DC evaluation accuracy.

Input/mA	Output/mV	Relative error
-100	-100.068	0.068%
-90	-90.014	0.016%
-80	-80.016	0.020%
-70	-69.983	0.024%
-60	-59.985	0.025%
-50	-50.023	0.046%
-40	-40.029	0.073%
-30	-30.021	0.070%
-20	-20.020	0.10%
-10	-10.013	0.13%
10	10.011	0.11%
20	20.023	0.12%
30	30.018	0.06%
40	40.031	0.078%
50	50.017	0.034%
60	60.015	0.025%
70	70.011	0.016%
80	80.022	0.028%
90	90.020	0.022%
100	99.937	0.063%

TABLE 3. AC (60 Hz) evaluation accuracy.

Input/mA	Output/mV	Relative error
10	10.021	0.21%
20	20.043	0.22%
30	30.022	0.073%
40	40.023	0.058%
50	49.974	0.052%
60	59.982	0.030%
70	69.988	0.017%
80	79.952	0.060%
90	90.050	0.056%
100	99.946	0.054%

C. LINEARITY AND ACCURACY EVALUATION

Based on the AC and DC residual currents used for the linearity assessment, we used the Fluke Standard Source 5730A to apply the AC/DC currents and measured the signals with the Fluke 8508 meter. The DC linearity and AC linearity are shown in Fig 14, respectively. The evaluation results show that the sensor has good linearity.

As can be seen from Tables 2,3 and 4, the sensor's DC evaluation accuracy is better than ±0.2%, AC (60 Hz) Evaluation accuracy is better than ±0.3%, and the AC evaluation accuracy is better than ±5%(20 kHz), achieving a highly accurate measurement of the residual current.

As for comparison, a commercial fluxgate current sensor, which is specially designed for the high-frequency residual currents of 100 kHz, has an AC accuracy of ±5%(< 10 kHz) and a DC accuracy of ±4% [36]. By contrast, the accuracy of the residual current sensor in this paper is significantly better than the commercial sensor.

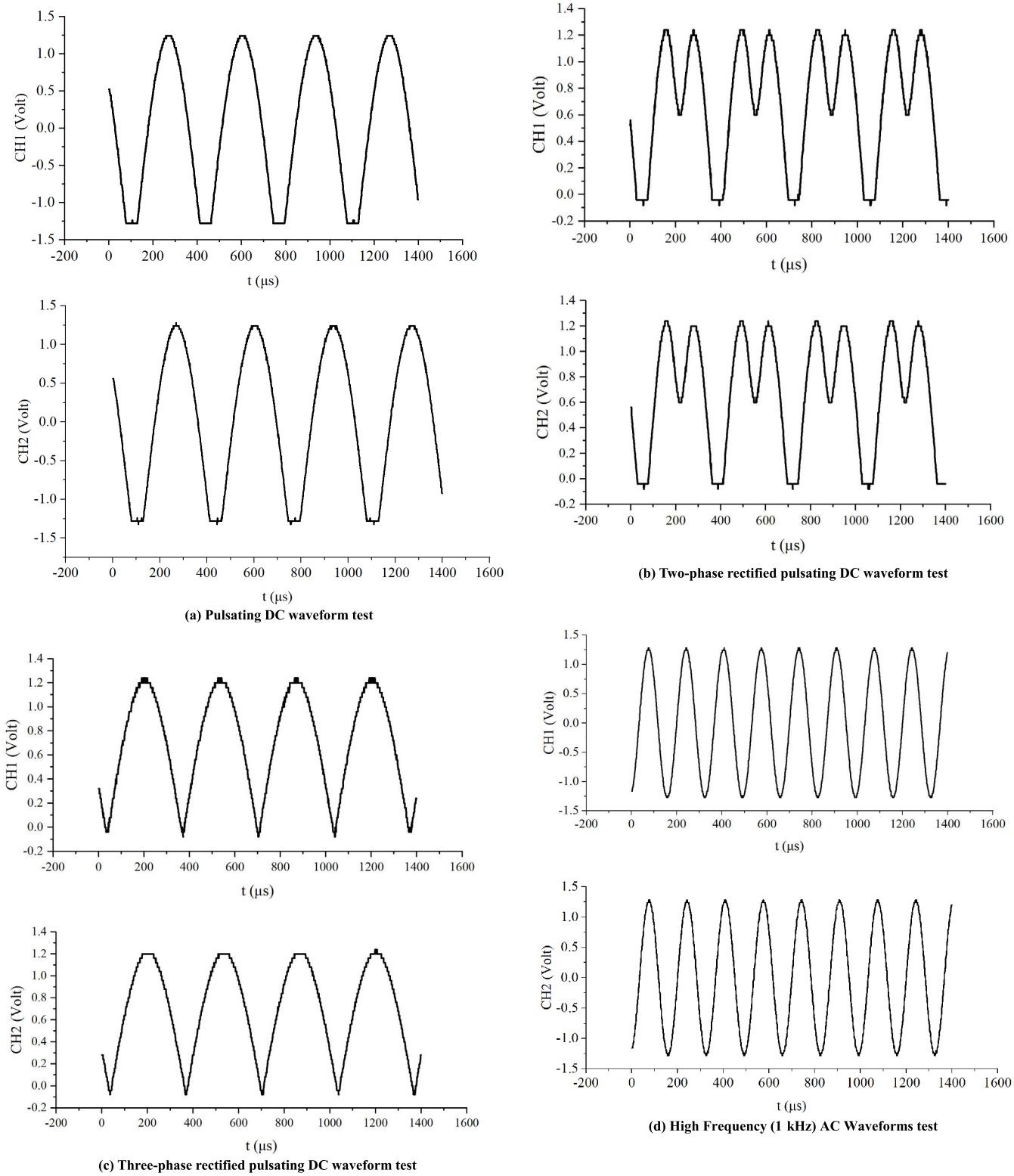

FIGURE 12. Pulsating DC residual current, two-phase rectified pulsating DC, Three-phase rectified pulsating DC residual current and high-frequency AC residual current waveform tests in (a), (b),(c),(d). CH1 - Measured current signal, CH2 - Sensor Output Signal.

D. SENSOR ZERO-POINT DYNAMIC CHANGE EVALUATION

The zero-point variation of the sensor is represented by a Fluke 8508 microvoltmeter, which records the change of zero-point after power-up. The results of multiple measurements are shown in Fig.15: the standard deviation is 0.00046 mA, the average value is 0.0006 mA, and

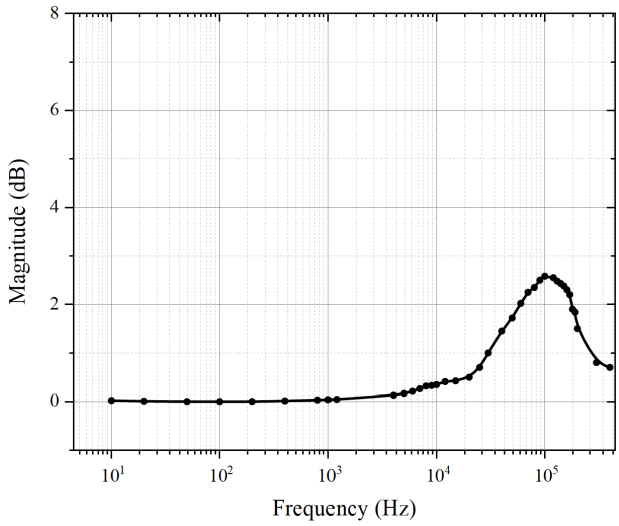

FIGURE 13. The amplitude frequency response of the proposed sensor measured in experiment. The black dots are experimental data, and the black curve through the dots is the fit of data.

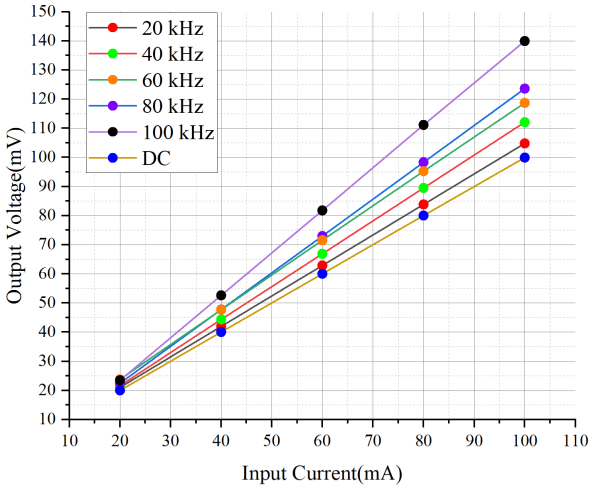

FIGURE 14. Sensor linearity. Blue dots, red dots, green dots, orange dots, purple dots, and black dots are experimental data, and each corresponding line is a linear fit.

TABLE 4. AC (20 kHz) evaluation accuracy.

Input/mA	Output/mV	Relative error
10	10.478	4.8%
20	20.808	4.0%
30	31.402	4.7%
40	41.550	3.9%
50	51.891	3.8%
60	62.575	4.3%
70	73.518	5.0%
80	81.845	4.8%
90	94.432	4.9%
100	104.395	4.4%

Δ_{max}=0.0014 mA, which is stable enough for currents within the range.

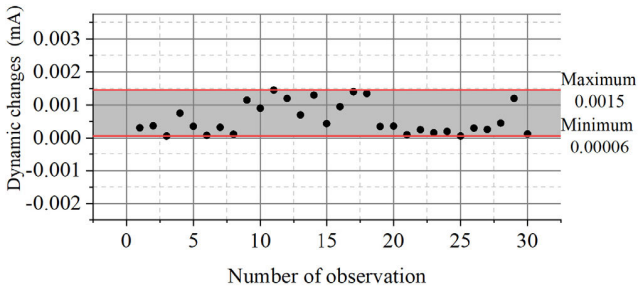

FIGURE 15. Zero-point dynamics. The grey fill is the distribution region of the zero-points under different time of observation, and the two red parallel lines represent the maximum and minimum zero-point change.

TABLE 5. Comparison of performance parameters.

Model	Accuracy	Zero-point change	Bandwidth	Production cost
A commercial fluxgate current sensor	±4%(DC) ±5%(10 kHz)	±0.2 mA	100 kHz	> 100 dollars.
The designed sensor	±0.2%(DC) ±5.0%(20 kHz)	±0.0014 mA	>100 kHz	About 30 dollars.

By contrast, a commercial fluxgate current sensor specifically designed for 100 kHz residual currents has a zero-point variation range of 0.2 mA [36]. The residual current sensor designed in this paper has a more stable zero point than it.

A comparison of comprehensive performance parameters is listed in Table 5.

IV. CONCLUSION

This paper presents a closed-loop residual current sensor based on self-excited oscillating fluxgate, which achieves high accuracy measurement of high-frequency residual current, by implementing the excitation voltage regulation module and increasing the AC winding. A prototype has been fabricated to verify the proposed scheme through experimental evaluation. The experimental results show that the DC measurement accuracy of the sensor is better than ±0.2%, AC (60 Hz) Evaluation accuracy is better than ±0.3%, and the AC evaluation accuracy is better than ±5%(20 kHz). In addition, the sensor bandwidth is over 100 kHz, and the standard deviation is 0.00046 mA based on multiple measurements of the zero-point dynamic change. The sensor we design has good stability to complex residual current waveforms in high-frequency power systems, which conforms to the IEC/TR 60755 and IEC 62752 standards. Compared with the typical high-frequency fluxgate residual current sensor, the proposed sensor has higher accuracy under milliamperes leakage current condition, simpler RC demodulation circuit, low cost and broader bandwidth. Our sensor meets the demand of high frequency residual current measurement in the performance evaluation of inverter motors, which are commonly used in the fields of new energy vehicles, wind energy storage and smart factories.

REFERENCES

[1] R. M. Tallam, S. B. Lee, G. C. Stone, G. B. Kliman, J. Yoo, T. G. Habetler, and R. G. Harley, "A survey of methods for detection of stator-related faults in induction machines," *IEEE Trans. Ind. Appl.*, vol. 43, no. 4, pp. 920–933, 2007.

[2] J. Rodriguez, J. Pontt, C. Silva, R. Musalem, P. Newman, R. Vargas, and S. Fuentes, "Resonances and overvoltages in a medium-voltage fan motor drive with long cables in an underground mine," *IEEE Trans. Ind. Appl.*, vol. 42, no. 3, pp. 856–863, May 2006.

[3] S. Bin Lee, K. Younsi, and G. B. Kliman, "An on-line technique for monitoring the insulation condition of AC machine stator windings," in *Proc. IEEE Int. Conf. Electr. Mach. Drives*, Mar. 2005, pp. 286–294.

[4] H. Xiao and S. Xie, "Leakage current analytical model and application in single-phase transformerless photovoltaic grid-connected inverter," *IEEE Trans. Electromagn. Compat.*, vol. 52, no. 4, pp. 902–913, Nov. 2010.

[5] K. Li, F. Niu, Y. Wu, Y. Wang, Y. Dai, L. Wang, and E. Li, "Nonlinear current detection based on magnetic modulation technology," *IEEE Trans. Magn.*, vol. 51, no. 11, pp. 1–4, Nov. 2015.

[6] P. Ripka, "Electric current sensors: A review," *Meas. Sci. Technol.*, vol. 21, no. 11, Nov. 2010, Art. no. 112001.

[7] S. Ziegler, R. C. Woodward, H. H.-C. Iu, and L. J. Borle, "Current sensing techniques: A review," *IEEE Sensors J.*, vol. 9, no. 4, pp. 354–376, Apr. 2009.

[8] S.-K. Lim, H.-S. Lee, H.-R. Cha, and S.-J. Park, "Multi-level DC/DC converter for E-mobility charging stations," *IEEE Access*, vol. 8, pp. 48774–48783, 2020.

[9] M. Tabari and A. Yazdani, "Stability of a DC distribution system for power system integration of plug-in hybrid electric vehicles," *IEEE Trans. Smart Grid*, vol. 5, no. 5, pp. 2564–2573, Sep. 2014.

[10] R. Li and F. Shi, "Control and optimization of residential photovoltaic power generation system with high efficiency isolated bidirectional DC–DC converter," *IEEE Access*, vol. 7, pp. 116107–116122, 2019.

[11] M. Starke, L. M. Tolbert, and B. Ozpineci, "AC vs. DC distribution: A loss comparison," in *Proc. IEEE/PES Transmiss. Distrib. Conf. Expo.*, Apr. 2008, pp. 1–7.

[12] M. C. Bastos, G. Fernqvist, G. Hudson, J. Pett, A. Cantone, F. Power, A. Saab, B. Halvarsson, and J. Pickering, "High accuracy current measurement in the main power converters of the large hadron collider: Tutorial 53," *IEEE Instrum. Meas. Mag.*, vol. 17, no. 1, pp. 66–73, Feb. 2014.

[13] K. Ding, W. Wang, and L. Xu, "Design and implementation of magnetic modulation DC leakage current transformer," *Inf. Technol.*, vol. 136, no. 3, pp. 131–133, 2014.

[14] J. Qi, G. Yang, and Z. Luo, "Error analysis of phase difference magnetic modulation DC leakage current sensor," *Automat. Instrum.*, vol. 38, no. 9, pp. 149–152, 2018.

[15] Z. Xie, D. Zhang, and N. Chen, "Simulation research of magnetic modulation sensor based on Fe based nanocrystalline," *Elect. Meas. Instrum.*, vol. 55, no. 18, pp. 125–130, 2018.

[16] L. Wang, X. Wang, and Z. Feng, "A simplified design and experimental verification of the magnetic modulation sensor based on half wave excitation signals," *Chin. J. Sensors Actuators*, vol. 28, no. 10, pp. 1448–1453, 2015.

[17] S. Wang, H. Li, Q. Liu, Q. Huang, and Y. Liu, "Design of a DC residual current sensor based on the improved DC component method," in *Proc. IEEE Power Energy Soc. Gen. Meeting (PESGM)*, Montreal, QC, Canada, Aug. 2020, pp. 1–5.

[18] G. Velasco-Quesada, M. Román-Lumbreras, A. Conesa-Roca, and F. Jeréz, "Design of a low-consumption fluxgate transducer for high-current measurement applications," *IEEE Sensors J.*, vol. 11, no. 2, pp. 280–287, Feb. 2011.

[19] N. Luo, F. Yang, Y. Zhang, and S. Li, "Experimental research on over-range measurement method based on quasi-digital direct-current leakage current sensor," *IEEE Access*, vol. 9, pp. 38934–38942, 2021.

[20] X. Yang, W. Guo, C. Li, B. Zhu, T. Chen, and W. Ge, "Design optimization of a fluxgate current sensor with low interference," *IEEE Trans. Appl. Supercond.*, vol. 26, no. 4, pp. 1–5, Jun. 2016.

[21] X. Zeliang, M. Yingzong, D. Feng, Z. Yue, and M. Anheuser, "Type B RCD with a simplified magnetic modulation/demodulation method," in *Proc. IEEE 6th Int. Power Electron. Motion Control Conf.*, May 2009, pp. 769–772.

[22] T. Kudo, S. Kuribara, and Y. Takahashi, "Wide-range AC/DC earth leakage current sensor using fluxgate with self-excitation system," in *Proc. IEEE SENSORS*, Oct. 2011, pp. 512–515.

[23] N. Wang, Z. Zhang, Z. Li, Q. He, F. Lin, and Y. Lu, "Design and characterization of a low-cost self-oscillating fluxgate transducer for precision measurement of high-current," *IEEE Sensors J.*, vol. 16, no. 9, pp. 2971–2981, May 2016.

[24] M. M. Ponjavic and R. M. Duric, "Nonlinear modeling of the self-oscillating fluxgate current sensor," *IEEE Sensors J.*, vol. 7, no. 11, pp. 1546–1553, Nov. 2007.

[25] T. R. Oliveira, "Design of a low-cost residual current sensor for LVDC power distribution application," in *Proc. 13th IEEE Int. Conf. Ind. Appl. (INDUSCON)*, Nov. 2018, pp. 1313–1319.

[26] D. Grybos, J. Leszczynski, C. Swieboda, M. Kwiecien, R. Rygal, M. Soinski, and W. Pluta, "Magnetic properties of composite cores made of nanocrystalline material for high frequency inductors and transformers," in *Proc. Innov. Mater. Technol. Electr. Eng. (i-MITEL)*, Sulecin, Poland, Apr. 2018, pp. 1–6.

[27] *VITROVAC 6025 En_Preliminary*, VACUUMSCHMELZE GmbH & Co. KG., Hanau, Germany, 2013.

[28] T. Wei-Hao, L. Yi, and W. Xiang-Jun, "Design of probe parameters for large-aperture open-close fluxgate current sensor," *Instrum. Technol. Sensors*, no. 12, pp. 25–33, 2022.

[29] I. M. Filanovsky and L. Taylor, "Circuit with nonlinear transformer allowing DC current measurements via an isolation gap," in *Proc. 35th Midwest Symp. Circuits Syst.*, Washington, DC, USA, Aug. 1998, pp. 318–323.

[30] P. Pejovic, "A simple circuit for direct current measurement using a transformer," *IEEE Trans. Circuits Syst. I, Fundam. Theory Appl.*, vol. 45, no. 8, pp. 830–837, Jan. 1998.

[31] S. Signell and K. Mossberg, "Design of high-frequency active RC-filters using passive compensation methods," in *Proc. IEEE Int. Symp. Circuits Syst.*, Espoo, Finland, Jun. 1988, pp. 2669–2672.

[32] P. Bowron, "Dynamic-range optimisation of second-order integrator-loop active filters," in *Proc. IEE 16th Saraga Colloq. Digit. Analogue Filters Filtering Syst.*, London, U.K., 1996, p. 13.

[33] Z. Han, "An applied study on the frequency characteristics of high-frequency current sensors," *Electrotechnology*, vol. 33, no. 1, pp. 45–47, 2012.

[34] *General Requirements for Residual Current Operated Protective Devices*, document IEC TR 60755, 2008.

[35] *In-Cable Control and Protection Device for Mode 2 Charging of Electric Road Vehicles (IC-CPD)*, document IEC62752, 2016.

[36] DANNISENSE. (2023). *RCMH070IB_v10*. [Online]. Available: https://danisense.com/products/residual-current-monitoring/

ZHIWEN DING was born in China, in 1998. He received the bachelor's degree from the Hefei University of Technology, in 2021. He is currently pursuing the master's degree with the National Institute of Metrology (NIM), Beijing, China. His current research interests include high current measurement and fluxgate current sensors.

JIAFU WANG (Member, IEEE) was born in Harbin, China, in 1983. He received the B.E. and Ph.D. degrees in electrical engineering from Tsinghua University, Beijing, China, in 2006 and 2012, respectively. From 2012 to 2015, he was a Postdoctoral Researcher with Tsinghua University. Since 2015, he has been an Associate Research Fellow with the National Institute of Metrology, Beijing. His current research interest includes the metrology technologies on ac and dc high voltage.

CHUANSHENG LI was born in 1984. He received the B.S. degree in instrument science and technology from the China University of Mining and Technology, Beijing, China, in 2006, and the Ph.D. degree in optical engineering from Beihang University, Beijing, in 2013. He began his metrology work with the National Institute of Metrology, Beijing, in 2015. His current research interests include wide-band large current metrology technology and fiber-optic current sensing technology.

KUN WANG (Member, IEEE) received the Ph.D. degree in precision instruments and machinery from Beihang University, Beijing, China, in 2023. He is currently a Postdoctoral Research Fellow with the National Institute of Metrology (NIM), Beijing. His current research interests include precision current measurement and metrology.

HAIMING SHAO (Member, IEEE) was born in 1965. He received the degree from the China Metrology Institute, Hangzhou, China, in 1987, and the M.S. and Ph.D. degrees from Tianjin University, Tianjin, China, in 1995 and 2010, respectively. He had been working on the development and investigation of dc resistance measurement standards after he joined the National Institute of Metrology (NIM), Beijing, China, where he began his metrology study career. He is currently in charge of the establishment of high-voltage and current standards.